

Detecting and Focusing on a Nonlinear Target in a Complex Medium

Antton Goicoechea,^{1,*} Jakob Hüpfel,² Stefan Rotter,² François Sarrazin,¹ and Matthieu Davy^{1,†}

¹Université de Rennes, CNRS, IETR - UMR 6164; F-35000 Rennes, France

²Institute for Theoretical Physics, Vienna University of Technology (TU Wien), A-1040 Vienna, Austria

(Dated: July 12, 2024)

Wavefront shaping techniques allow waves to be focused on a diffraction-limited target deep inside disordered media. To identify the target position, a guidestar is required that typically emits a frequency-shifted signal. Here we present a noninvasive matrix approach operating at a single frequency only, based on the variation of the field scattered by a nonlinear target illuminated at two incident powers. The local perturbation induced by the nonlinearity serves as a guide for identifying optimal incident wavefronts. We demonstrate maximal focusing on electronic devices embedded in chaotic microwave cavities and extend our approach to temporal signals. Finally, we exploit the programmability offered by reconfigurable smart surfaces to enhance the intensity delivered to a nonlinear target. Our results pave the way for deep imaging protocols that use any type of nonlinearity as feedback, requiring only the measurement of a monochromatic scattering matrix.

Introduction.—Wavefront shaping techniques can partially counteract the effect of disorder by coherently controlling wave-matter interaction [1–3]. Of particular interest is the possibility to focus waves on a diffraction-limited focal spot inside or behind a strongly scattering medium [4] or to deposit energy to a target region [5, 6]. In the linear regime, when the field at the target location is directly accessible, the incident wavefront for focusing can be optimally tailored in space and/or time using techniques such as phase-conjugation for monochromatic waves [7–10], time reversal for broadband signals [11] or the eigenstates of an operator constructed from the scattering matrix [6, 12, 13]. However, embedding a detector within a scattering medium is an invasive procedure that rules out many applications in deep optical imaging, wireless communications, wireless power transfer, or sensing. Noninvasive approaches therefore rely on the presence of a guidestar within the medium [3, 9, 14–16].

The nonlinear wave-matter interaction has emerged in this context as an efficient approach for deep imaging. Nonlinear techniques rely on the localized feedback generated by a nonlinear target. In acoustics, microbubbles serve as contrast agents for ultrasound imaging [17, 18] while in optics, Raman microscopy [19], two-photon fluorescence [20] or second-harmonic generation [21, 22] have been exploited to obtain a diffraction-limited focal spot [16, 23]. In the microwave regime, most electronic devices, even as simple as a diode [24–26], exhibit a nonlinear behavior and can be detected by harmonic radars in cluttered environments [27, 28]. All these techniques nevertheless require complex experimental setups to detect and/or filter the frequency-shifted nonlinear signal.

A local perturbation of a linear scattering medium can also serve as a guidestar [29–35]. Any change within a disordered sample is encoded in the random speckle pattern resulting from the complex interaction of the incident wave and the sample [36]. Therefore, the derivative of the scattering matrix $S(\omega)$ with respect to a parameter θ , i.e. $\partial_\theta S$, contains information about θ . For unitary

scattering matrices, the eigenvalues of the generalized Wigner-Smith (WS) operator $Q = -iS^{-1}\partial_\theta S$ indicate how strongly the conjugate quantity to θ is affected by a variation [29, 30, 37]. The operator $(\partial_\theta S)^\dagger \partial_\theta S$ also turns out to measure the content of Fisher information carried by the scattered wave on the parameter θ [32, 38, 39]. The eigenstates of these operators thus provide the solution for maximal focusing, micromanipulation or for optimal sensitivity with respect to θ . However, setting up these operators requires a variation of the target parameter(s), which is impossible in linear static systems without invasive external intervention inside the scattering medium.

Here, we present a noninvasive approach for optimal focusing on a nonlinear target in static scattering systems. Most importantly, our approach does not require a measurement of the harmonic response of the target device, it allows the detection of all types of nonlinearities, and it does not rely on prior knowledge on the medium or on the target. All these requirements are satisfied by leveraging the nonlinear scattering response, which we probe by tuning the incident power [22, 40]. Specifically, we extract wavefronts focusing in space and time by measuring the response of the system for two incident powers and by filtering out the expected linear response. Theoretical results are confirmed by microwave measurements within scattering systems. Finally, we show that the intensity focused on the nonlinear target can be further enhanced in programmable environments by optimizing reconfigurable metasurfaces.

Theoretical analysis.—We consider a system made up of dielectric obstacles described by the dielectric function $\epsilon(\mathbf{r})$, which we probe by coherent monochromatic electromagnetic waves at frequency ω . Our objective is to find an incident state \mathbf{E}^{in} that creates an optimal focus on a nonlinear target embedded inside this scattering environment.

To disentangle the linear (L) from the nonlinear (NL) scattering response, we write the far field solution $\mathbf{E}_\omega^\alpha(\mathbf{r})$

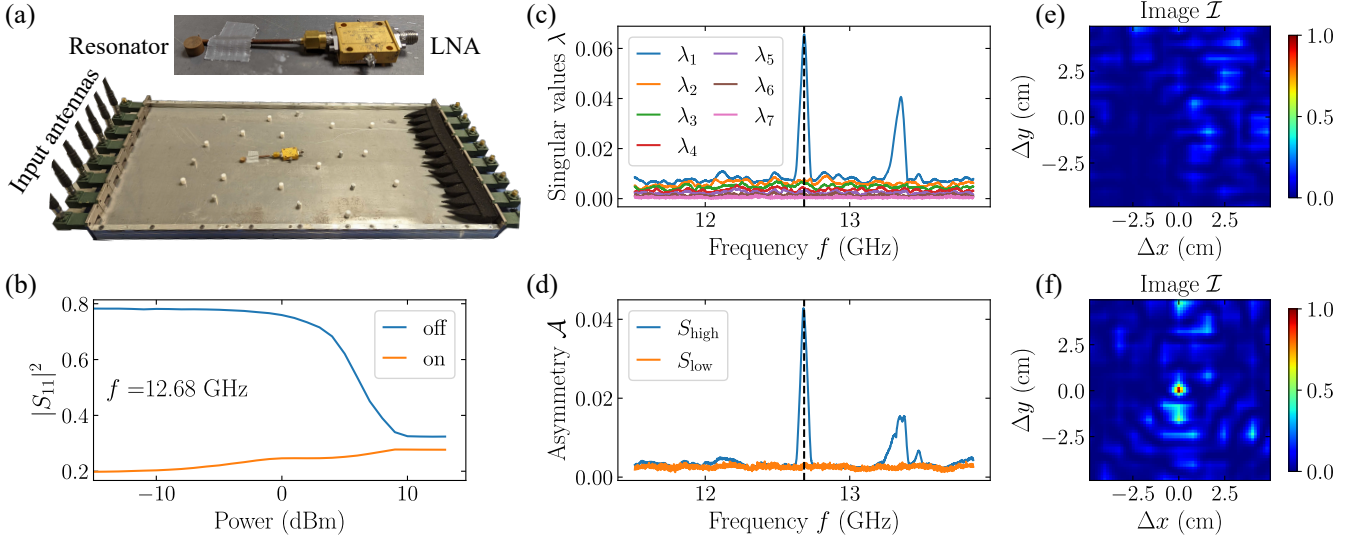


FIG. 1. (a) Photograph of the experimental setup. A resonator coupled in the near field to a wire antenna connected to a (nonlinear) low-noise amplifier (LNA) is located within a two-dimensional multimode waveguide (cover plate not shown). The scattering matrix is measured using seven antennas at the left interface. An absorbing foam is placed at the right interface to mimic open boundary conditions. (b) Reflection parameter $r = |S_{11}|^2$ of the LNA as a function of incident power P for an empty single-mode waveguide at $f_0 = 12.68$ GHz with the second port connected to the LNA (powered –‘on’ – or not – ‘off’ terminated by an open-circuit condition). (c,d) Spectra of the singular values λ_n of ΔS (c) and asymmetry factor \mathcal{A} (d). The nonlinearity is maximal at the resonance of the nonlinear target $f = f_0$ indicated by a black-dashed line. (e,f) Intensity map within the system for a random illumination (e) or with $\mathbf{c}^{\text{in}} = \mathbf{d}^*$ (f). Both maps are normalized by the maximum value obtained for the optimized wavefront.

for an incident amplitude α as follows:

$$\mathbf{E}_\omega^\alpha(\mathbf{r}) = \alpha \mathbf{E}_\omega^{\text{L}}(\mathbf{r}) + \int_{\mathbb{R}^3} d\mathbf{r}' G_\omega(\mathbf{r}, \mathbf{r}') \mathbf{P}_\omega^{\text{NL}}[\mathbf{E}^\alpha](\mathbf{r}'). \quad (1)$$

Here, $\mathbf{E}_\omega^{\text{L}}(\mathbf{r})$ describes the linear component of the field for normalized amplitude $\alpha = 1$, $\mathbf{P}_\omega^{\text{NL}}[\mathbf{E}^\alpha](\mathbf{r}')$ is the target’s nonlinear polarisation field and $G_\omega(\mathbf{r}, \mathbf{r}')$ is the Green’s tensor of the system without nonlinearities.

Note that both the linear response (the first term) of the system and the nonlinear response (the second term) are considered to be time-harmonic waves oscillating at the same frequency. The idea is now to eliminate the linear term and to time-reverse the nonlinear signal to create a focus at the target (see Supplementary Material [41] for details). We achieve this by varying the amplitude of the incident field by $\delta\alpha$, then the differential field $\delta\mathbf{E}_\omega(\mathbf{r}) = (\alpha + \delta\alpha)^{-1} \mathbf{E}_\omega^{\alpha + \delta\alpha}(\mathbf{r}) - \alpha^{-1} \mathbf{E}_\omega^\alpha(\mathbf{r})$ satisfies

$$\delta\mathbf{E}_\omega(\mathbf{r}) = \int_{\mathbb{R}^3} d\mathbf{r}' G_\omega(\mathbf{r}, \mathbf{r}') \delta\mathbf{P}_\omega^{\text{NL}}(\mathbf{r}'). \quad (2)$$

We see here that $\delta\mathbf{P}_\omega^{\text{NL}}(\mathbf{r}') = \mathbf{P}_\omega^{\text{NL}}[\mathbf{E}^{\alpha + \delta\alpha}](\mathbf{r}') - \mathbf{P}_\omega^{\text{NL}}[\mathbf{E}^\alpha](\mathbf{r}')$ acts as a source term for $\delta\mathbf{E}_\omega(\mathbf{r})$ with the coupling from the polarisation field to the far field being given by the Green’s tensor $G_\omega(\mathbf{r}, \mathbf{r}')$. This becomes especially apparent for a point-like nonlinearity located at \mathbf{r}_0 , where the differential field provides the exact coupling between the location of the nonlinearity to the far field,

i.e. $\delta\mathbf{E}_\omega(\mathbf{r}) \propto G_\omega(\mathbf{r}, \mathbf{r}_0)$. Thus, as long as the incident state interacts with the nonlinearity, the time-reversed of $\delta\mathbf{E}(\mathbf{r})$ provides a focus from the far field onto the nonlinear target. The focus that is created with this method is optimal for a given incident strength α in the case of weak point-like nonlinearities in a system with only a single polarisation degree of freedom, e.g. a thin waveguide as shown in Fig. 1 (a). Note that throughout the article, ‘optimal’ and ‘maximal’ refer to states obtainable in the linear regime because the nonlinearity is assumed to be weak (perturbative regime).

From now on, we focus on scalar waves. For linear systems, a comprehensive description of the connection between all input and all output channels (quantified by $\mathbf{c}^{\text{in}}, \mathbf{c}^{\text{out}}$, respectively) is provided by the linear scattering matrix, $\mathbf{c}^{\text{out}} = S^{\text{L}} \mathbf{c}^{\text{in}}$. However, due to the presence of the nonlinearity, the superposition principle no longer holds for incident fields that interact with $\mathbf{P}_\omega^{\text{NL}}$. On the other hand, incident states that avoid the nonlinearity preserve this property. We exploit this by splitting the incident modes into a part that behaves linearly and a nonlinear part. For this, we describe the Green’s function $G_\omega(\mathbf{r}, \mathbf{r}_0)$ in the basis of the output channels (quantified by \mathbf{d} , i.e. $\mathbf{c}^{\text{out}} = \mathbf{d}$). The Green’s identity now tells us that all incident fields \mathbf{c}^{in} that are perpendicular to \mathbf{d}^* do not interact with the nonlinearity. This makes it possible to introduce a correction to the relation between the

incident and outgoing fields

$$\mathbf{c}^{\text{out}} = S^{\text{L}}\mathbf{c}^{\text{in}} + \alpha^{-1}\mathbf{d}f[\mathbf{d} \cdot \mathbf{c}^{\text{in}}], \quad (3)$$

where f is a nonlinear function (see Supplementary Material [41]). If we now probe the system with basis states \mathbf{e}_n of incident modes at a given input power α , the resulting input-output relation can be expressed through the following power-dependent scattering matrix

$$S_{m,n}^{\alpha} = S_{m,n}^{\text{L}} + \alpha^{-1}d_m f[\alpha d_n], \quad (4)$$

where $S_{m,n}^{\alpha}$ corresponds to the output in mode \mathbf{e}_m for an input in mode \mathbf{e}_n . However, it is important to note that S^{α} is not a conventional scattering matrix. While it describes the scattering for the set of incident states at a given power, it cannot encompass the full nonlinear nature of Eq. (3).

Nevertheless, S^{α} can now be used to identify the optimal focusing state by using the differential matrix

$$\begin{aligned} \Delta S_{m,n} &= S_{m,n}^{\alpha+\delta\alpha} - S_{m,n}^{\alpha} \\ &= d_m [(\alpha + \delta\alpha)^{-1}f[(\alpha + \delta\alpha)d_n] - \alpha^{-1}f[\alpha d_n]]. \end{aligned} \quad (5)$$

The rank of the matrix is equal to the number of point-like nonlinearities (here one), each coupling to the far field through a unique incident wavefront. \mathbf{d} can now be estimated by applying a singular value decomposition (SVD) on $\Delta S = U\lambda V^*$. The left singular vector \mathbf{U}_1 of the largest singular value λ_1 corresponds to \mathbf{d} . By applying a phase-conjugation, the incident wavefront \mathbf{d}^* provides maximal focusing onto the target.

The nonlinear scattering coefficient of the target depends on the field $E_n(r_0)$ transmitted by channel n . In the absence of global symmetries, we have $E_n(r_0) \neq E_m(r_0)$ in general for $n \neq m$. In contrast to linear systems with modulation of an antenna impedance or dielectric permittivity of a subwavelength object [30, 31, 34, 35], the right and left singular vector of ΔS are therefore not equal.

Experimental results.—In our first experiment, we consider a nonlinear target embedded within a two-dimensional scattering system working in the microwave range. The target consists of a high-Q dielectric cylinder with a refraction index of $n \approx 6$ coupled in its near field to a wire antenna connected to a low-noise amplifier (LNA). This nonlinear passive target - the LNA is not powered - is conceptually similar to the coupling of a resonator to a short-circuited diode found in Refs [24–26] for nonlinear coherent perfect absorption or the formation of defect modes. However, we find that our target exhibits a more pronounced nonlinearity due to the presence of transistors in the LNA. This is crucial since the target is excited from its far field. We characterize the reflectivity of the LNA by connecting it to a single-mode waveguide whose reflection parameter $|r(\omega)|^2 = |S_{11}|^2$ is

measured for increasing input power P . While $|r(\omega)|^2$ is constant at low powers indicating a linear behaviour, we observe in Fig. 1(b) that $|r(\omega)|^2$ rapidly decreases for $P > 0$ dBm before saturating for $P > 10$ dBm. The nonlinearity therefore results from enhanced absorption within the LNA at high power.

The nonlinear target is then placed within a multi-mode waveguide (cavity) supporting a single mode in its vertical direction between 12 GHz and 15 GHz [42, 43]. Seven metallic and 13 dielectric scatterers are randomly placed inside the cavity to randomize the field. The flux-normalized matrix $S^{\alpha}(\omega)$ is measured using a vector network analyzer (VNA) between $N = 7$ single-mode waveguides that are connected to the left interface of the cavity by coax-to-waveguide transitions. At the right interface, we place an absorbing foam to mimic open boundary conditions. The differential matrix $\Delta S(\omega)$ is constructed from measurements of $S^{\alpha}(\omega)$ at two incident powers $P_1 = 0$ dBm ($S = S^{\text{L}}$) and $P_2 = 12$ dBm.

Two peaks on the spectrum of the first singular value $\lambda_1(\omega)$ of ΔS are observed at 12.68 and 13.35 GHz in Fig. 1(c), corresponding to resonances of the high-Q dielectric cylinder. The enhancement of the field intensity within the cylinder at resonance results in a strong coupling with the LNA, and thereby increases nonlinear effects. We then scan the normalized field $t_n(x, y; \omega)$ inside the medium for each source channel n by translating a short wire antenna in holes drilled into the top plate of the cavity. These measurements allow us to reconstruct the intensity map $\mathcal{I}(x, y; \omega)$ for any arbitrary incident wavefront \mathbf{c}^{in} , $\mathcal{I}(x, y; \omega) = |\mathbf{c}^{\text{in}*}(\omega) \cdot \mathbf{t}(x, y; \omega)|^2$. For the phase-conjugate of the first singular vector $\mathbf{c}^{\text{in}} = \mathbf{d}^*$, a strong enhancement of the intensity at the resonance ω_n is observed in Fig. 1(f) compared to random illumination in Fig. 1(e), as expected since \mathbf{d} gives the vector of Green's functions between the sources and the target. The intensity at the focus at 12.68 GHz is enhanced on average by a factor $\eta \simeq 4.7$ relative to a random incident wavefront.

Whereas we probed the system at two incident powers in order to apply a focus onto a target, we can instead exploit the reciprocity of linear systems for the detection of the nonlinearity. For linear systems, the scattering matrix is symmetric; however, the nonreciprocity induced by the nonlinearity breaks the symmetry of S^{α} [44–46], i.e.

$$(S^{\alpha} - (S^{\alpha})^T)_{m,n} = d_m \alpha^{-1} f(\alpha d_n) - d_n \alpha^{-1} f(\alpha d_m). \quad (6)$$

Thus, detecting the presence of a nonlinearity in practice requires a single measurement of $S(\omega)$ at high power by measuring the norm of the asymmetric part

$$\mathcal{A} = \|S^{\alpha} - (S^{\alpha})^T\|_F, \quad (7)$$

where $\|\cdot\|_F$ represents the Frobenius norm. At low power, $\mathcal{A}(\omega)$ is dominated by the noise level as the system is operating in the linear regime (see Fig. 1(d)). However, at

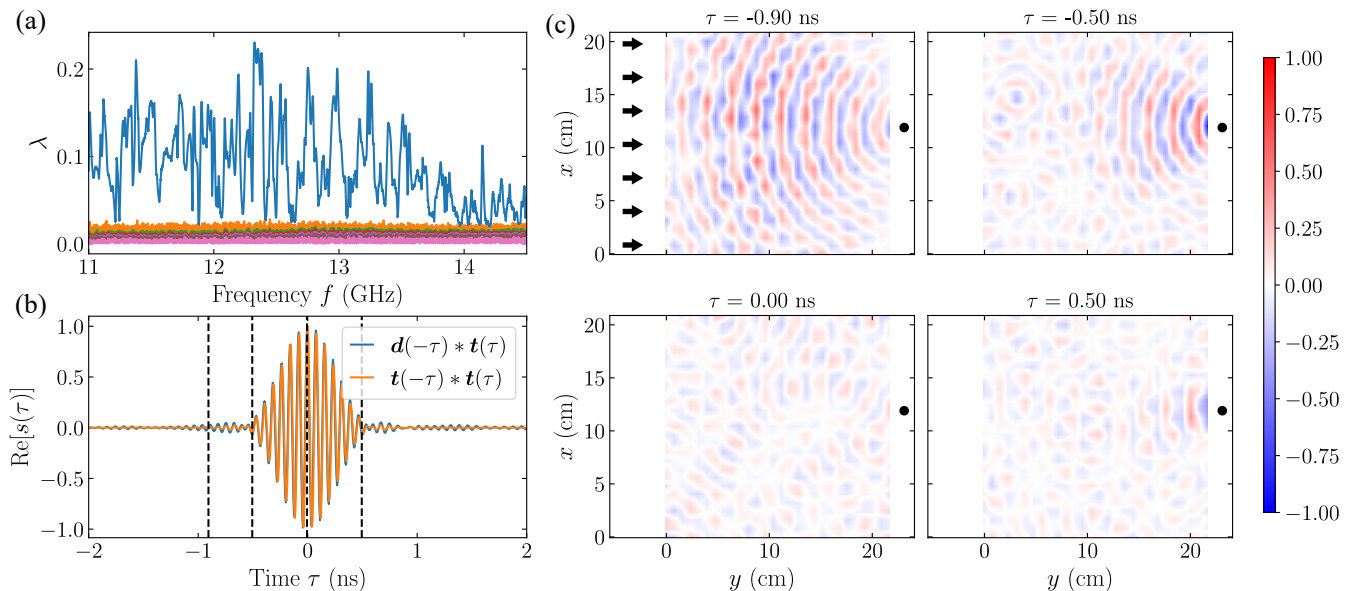


FIG. 2. Experimental results for a powered LNA connected to a single mode coax-to-waveguide transition located at the right interface of the cavity. (a) Spectrum of singular values λ_n . (b) Temporal signal at the nonlinear target corresponding to the back-propagation of the reconstructed signal for maximal focusing in space and time (blue line) and to a time-reversal experiment (orange line). The ratio of maximum amplitudes between them is 0.96. (c) Real parts of the field at four times indicated by black dashed lines in (b) obtained from back-propagating \mathbf{d}^* . The field around the position of the target (black dot) could not be probed since the port is located outside the cavity. The input antennas (indicated by black arrows) are located 30 cm toward the left of the map.

high power, $\mathcal{A}(\omega)$ exhibits similar resonances as $\lambda_1(\omega)$. Note that this reciprocity condition is not completely able to extract \mathbf{d} . More specifically, an SVD of the rank-two matrix $S^\alpha - (S^\alpha)^T$ provides us with the vector space spanned by \mathbf{d} and $[f(\alpha d_n)]_n$. However, it is in general not possible to separate these states from each other without further measurements. Furthermore, \mathcal{A} cannot give an indication on the number of nonlinearities within the system, only that nonlinear interactions have taken place.

We now demonstrate spatio-temporal focusing on a nonlinear target. The absorbing foams shown in Fig. 1 are removed and the LNA is connected (without the resonator) to a single-mode waveguide located at the right interface. Apart from the nonlinear target, the cavity is now closed as the antennas at the right interface are terminated by open circuits (making them reflectors). The LNA is now powered so that the transmission coefficient $\mathbf{t}(\omega)$ to the target can also be measured by connecting the LNA to the eighth channel of the VNA. This is done only for the purpose of comparison as the measurement of $\mathbf{t}(\omega)$ is not necessary to determine the incident waveform. The nonlinearity is nonresonant as the antennas are matched over a broad frequency range (see Fig. 2(a)). Fluctuations in $\lambda_1(\omega)$ arise from multiple scattering within the cavity.

Although the spatial wavefront for optimal focusing $\mathbf{e}^{\text{in}}(\omega) = \mathbf{d}^*(\omega)$ is obtained at each frequency through an SVD, the global phase $\phi(\omega)$ for optimal temporal focus-

ing is still unknown. We determine $\phi(\omega)$ using the procedure described in Ref. [34] that aligns the phase of each frequency component at the focal point (see Supplemental Material [41]). The temporal signals found from the inverse Fourier transform $s_{\text{opt}}(\tau) = \text{FT}^{-1}[\mathbf{e}^{\text{opt}}(\omega) \cdot \mathbf{t}(\omega)]$ and $s(\tau) = \text{FT}^{-1}[\mathbf{t}^*(\omega) \cdot \mathbf{t}(\omega)]$ are in excellent agreement with each other, as shown in Fig. 2(b), demonstrating maximal focusing both in time and space on the nonlinear target. The back-propagated signals within the cavity $\mathcal{I}(x, y; \tau) = \text{FT}^{-1}[\mathbf{e}^{\text{in}*} \cdot \mathbf{t}(x, y; \omega)]$ are presented in Fig. 2(c). Interestingly, the amplitude of the outgoing field at positive times is strongly reduced relative to the incident field at negative times in Fig. 2(c-d), which indicates strong absorption within the lossy nonlinear target.

In open environments for which the energy density illuminating a target is smaller than in confined geometries, wavefront shaping techniques may not be sufficient to detect the nonlinear signal. We thus investigate how the environment can be tuned to enhance the signal at the target [31, 47, 48]. For this purpose, we study a three-dimensional enclosure made programmable using a reconfigurable intelligent surface (RIS) (see Fig. 3(a)). For each of the 304 meta-atoms of the RIS, two states with a phase difference of roughly π in reflection can be configured electronically. Seven antennas are used to measure a 7×7 scattering matrix in the spectral window between 4.8 GHz and 5.8 GHz. The eighth antenna is connected to the nonlinear powered LNA.

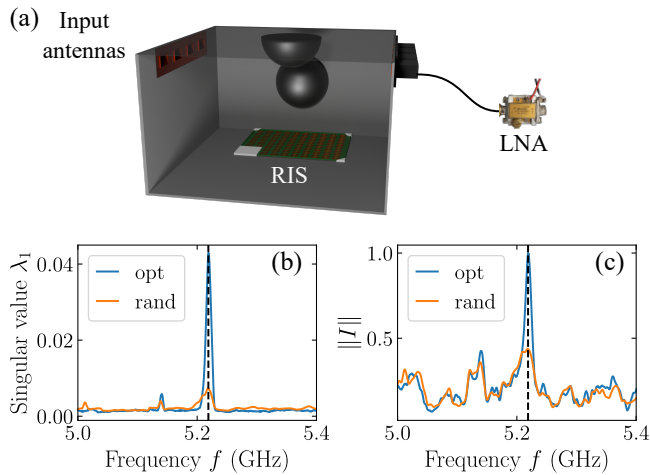


FIG. 3. (a) Schematic of the experiment. We measure the scattering matrix S of a chaotic cavity using $N = 7$ antennas. (b) Optimization result for $\lambda_1(f)$ compared with an average of 100 random configurations of the Reconfigurable Intelligent Surface (RIS). (c) Same as (b) for the intensity measured at the target's position.

The metasurface is first optimized iteratively to maximize the first singular value $\lambda_1(f)$ of ΔS at a single frequency $f_{\text{opt}} = 5.22$ GHz. This corresponds to a modification of the Green's function inside the system such that for the wavefront U_1 the intensity at the position of the nonlinear device is increased. The result is shown in Fig. 3 (b). At f_{opt} , the enhancement is 5.9 fold compared to the average value for random configurations. The optimization process also results in a strong enhancement of the asymmetry factor $\mathcal{A}(f_{\text{opt}})$ by a factor 3.5, and of the intensity at the target's position by a factor 2.3 (Fig. 3 (c)).

Conclusion.—We have demonstrated that nonlinear elements embedded in a complex medium can be detected and localized using measurements of the scattering matrix at a single frequency for two incident powers (no harmonic generation is required). We have shown that this noninvasive approach enables spatio-temporal focusing on nonlinear targets. Our approach is broadly applicable to any kind of wave and to any type of nonlinearity. Since smartphones contain nonlinear elements, this could provide a way to enhance the focusing of Wi-Fi signals on these devices in complex environments and may inspire new detection and localization setups.

This work is supported in part by the European Union through a European Regional Development Fund (ERDF), by the Ministry of Higher Education and Research, CNRS, Brittany region, Conseils Départementaux d'Ille-et-Vilaine and Côtes d'Armor, Rennes Métropole, and Lannion Trégor Communauté, through the CPER Project CyMoCod, in part by the French "Agence Nationale de la Recherche" (ANR) under Grant ANR-22-CPJ1-0070-01, and in part by the

Direction Générale de l'Armement through the Creach Labs under the project TRSweep. M.D. acknowledges the Institut Universitaire de France. The metasurface prototypes were purchased from Greenerwave. The authors acknowledge P. E. Davy for the 3D rendering of the experimental setup in Fig. 3(a).

* antton.goicoechea@univ-rennes.fr

† matthieu.davy@univ-rennes.fr

- [1] A. P. Mosk, A. Lagendijk, G. Lerosey, and M. Fink, Controlling waves in space and time for imaging and focusing in complex media, *Nature Photon* **6**, 283 (2012).
- [2] S. Rotter and S. Gigan, Light fields in complex media: Mesoscopic scattering meets wave control, *Rev. Mod. Phys.* **89**, 015005 (2017).
- [3] H. Cao, A. P. Mosk, and S. Rotter, Shaping the propagation of light in complex media, *Nat. Phys.* **18**, 994 (2022).
- [4] I. M. Vellekoop, A. Lagendijk, and A. P. Mosk, Exploiting disorder for perfect focusing, *Nature Photon* **4**, 320 (2010).
- [5] S. Jeong, Y.-R. Lee, W. Choi, S. Kang, J. H. Hong, J.-S. Park, Y.-S. Lim, H.-G. Park, and W. Choi, Focusing of light energy inside a scattering medium by controlling the time-gated multiple light scattering, *Nature Photon* **12**, 277 (2018).
- [6] N. Bender, A. Yamilov, A. Goetschy, H. Yilmaz, C. W. Hsu, and H. Cao, Depth-targeted energy delivery deep inside scattering media, *Nat. Phys.* **18**, 309 (2022).
- [7] Z. Yaqoob, D. Psaltis, M. S. Feld, and C. Yang, Optical phase conjugation for turbidity suppression in biological samples, *Nature Photon* **2**, 110 (2008).
- [8] S. M. Popoff, G. Lerosey, R. Carminati, M. Fink, A. C. Boccara, and S. Gigan, Measuring the Transmission Matrix in Optics: An Approach to the Study and Control of Light Propagation in Disordered Media, *Phys. Rev. Lett.* **104**, 100601 (2010).
- [9] X. Xu, H. Liu, and L. V. Wang, Time-reversed ultrasonically encoded optical focusing into scattering media, *Nature Photon* **5**, 154 (2011).
- [10] C. W. Hsu, S. F. Liew, A. Goetschy, H. Cao, and A. D. Stone, Correlation-enhanced control of wave focusing in disordered media, *Nat. Phys.* **10**.1038/NPHYS4036 (2016).
- [11] A. Derode, P. Roux, and M. Fink, Robust Acoustic Time Reversal with High-Order Multiple Scattering, *Phys. Rev. Lett.* **75**, 4206 (1995).
- [12] M. Kim, Y. Choi, C. Yoon, W. Choi, J. Kim, Q.-H. Park, and W. Choi, Maximal energy transport through disordered media with the implementation of transmission eigenchannels, *Nature Photon* **6**, 581 (2012).
- [13] W. Lambert, L. A. Cobus, T. Frappart, M. Fink, and A. Aubry, Distortion matrix approach for ultrasound imaging of random scattering media, *Proc. Natl. Acad. Sci.* **117**, 14645 (2020).
- [14] B. Judkewitz, Y. M. Wang, R. Horstmeyer, A. Mathy, and C. Yang, Speckle-scale focusing in the diffusive regime with time reversal of variance-encoded light (TROVE), *Nature Photon* **7**, 300 (2013).
- [15] P. Lai, L. Wang, J. W. Tay, and L. V. Wang, Photoa-

- coustically guided wavefront shaping for enhanced optical focusing in scattering media, *Nature Photon* **9**, 126 (2015).
- [16] R. Horstmeyer, H. Ruan, and C. Yang, Guidestar-assisted wavefront-shaping methods for focusing light into biological tissue, *Nature Photon* **9**, 563 (2015).
- [17] D. Miller, Ultrasonic detection of resonant cavitation bubbles in a flow tube by their second-harmonic emissions, *Ultrasonics* **19**, 217 (1981).
- [18] S. Qin, C. F. Caskey, and K. W. Ferrara, Ultrasound contrast microbubbles in imaging and therapy: Physical principles and engineering, *Phys. Med. Biol.* **54**, R27 (2009).
- [19] C. L. Evans and X. S. Xie, Coherent Anti-Stokes Raman Scattering Microscopy: Chemical Imaging for Biology and Medicine, *Annual Rev. Anal. Chem.* **1**, 883 (2008).
- [20] O. Katz, E. Small, Y. Guan, and Y. Silberberg, Noninvasive nonlinear focusing and imaging through strongly scattering turbid layers, *Optica* **1**, 170 (2014).
- [21] H. B. De Aguiar, S. Brasselet, and S. Gigan, Enhanced nonlinear imaging through scattering media using transmission-matrix-based wave-front shaping, *Phys. Rev. A* **94**, 043830 (2016).
- [22] J. Moon, Y.-C. Cho, S. Kang, M. Jang, and W. Choi, Measuring the scattering tensor of a disordered nonlinear medium, *Nat. Phys.* **19**, 1709 (2023).
- [23] S. Yoon, M. Kim, M. Jang, Y. Choi, W. Choi, S. Kang, and W. Choi, Deep optical imaging within complex scattering media, *Nat Rev Phys* **2**, 141 (2020).
- [24] M. Reisner, D. H. Jeon, C. Schindler, H. Schomerus, F. Mortessagne, U. Kuhl, and T. Kottos, Self-Shielded Topological Receiver Protectors, *Phys. Rev. Applied* **13**, 034067 (2020).
- [25] D. H. Jeon, M. Reisner, F. Mortessagne, T. Kottos, and U. Kuhl, Non-Hermitian C T -Symmetric Spectral Protection of Nonlinear Defect Modes, *Phys. Rev. Lett.* **125**, 113901 (2020).
- [26] S. Suwunnarat, Y. Tang, M. Reisner, F. Mortessagne, U. Kuhl, and T. Kottos, Non-linear coherent perfect absorption in the proximity of exceptional points, *Commun Phys* **5**, 5 (2022).
- [27] G. J. Mazzano, A. F. Martone, K. I. Ranney, and R. M. Narayanan, Nonlinear Radar for Finding RF Electronics: System Design and Recent Advancements, *IEEE Trans. Microwave Theory Techn.* **65**, 1716 (2017).
- [28] B. Perez, G. Mazzano, T. J. Pierson, and D. Kotz, Detecting the Presence of Electronic Devices in Smart Homes Using Harmonic Radar Technology, *Remote Sensing* **14**, 327 (2022).
- [29] P. Ambichl, A. Brandstötter, J. Böhm, M. Kühmayer, U. Kuhl, and S. Rotter, Focusing inside Disordered Media with the Generalized Wigner-Smith Operator, *Phys. Rev. Lett.* **119**, 033903 (2017).
- [30] M. Horodyski, M. Kühmayer, A. Brandstötter, K. Pichler, Y. V. Fyodorov, U. Kuhl, and S. Rotter, Optimal wave fields for micromanipulation in complex scattering environments, *Nat. Photonics* **14**, 149 (2020).
- [31] P. Del Hougne, K. B. Yeo, P. Besnier, and M. Davy, Coherent Wave Control in Complex Media with Arbitrary Wavefronts, *Phys. Rev. Lett.* **126**, 193903 (2021).
- [32] D. Bouchet, S. Rotter, and A. P. Mosk, Maximum information states for coherent scattering measurements, *Nat. Phys.* **17**, 564 (2021).
- [33] D. Bouchet and E. Bossy, Temporal shaping of wave fields for optimally precise measurements in scattering environments, *Phys. Rev. Research* **5**, 013144 (2023).
- [34] K. B. Yeo, C. Leconte, P. del Hougne, P. Besnier, and M. Davy, Time Reversal Communications With Channel State Information Estimated From Impedance Modulation at the Receiver, *IEEE Access* **10**, 91119 (2022).
- [35] J. Sol, L. L. Magoarou, and P. del Hougne, Optimal blind focusing on perturbation-inducing targets in sub-unitary complex media (2024), [arxiv:2401.15415](https://arxiv.org/abs/2401.15415) [physics].
- [36] R. Berkovits, Sensitivity of the multiple-scattering speckle pattern to the motion of a single scatterer, *Phys. Rev. B* **43**, 8638 (1991).
- [37] B. Orzabayev, M. Malléjac, N. Bachelard, S. Rotter, and R. Fleury, Wave-momentum shaping for moving objects in heterogeneous and dynamic media, *Nature Physics* , 1 (2024).
- [38] M. Horodyski, D. Bouchet, M. Kühmayer, and S. Rotter, Invariance Property of the Fisher Information in Scattering Media, *Phys. Rev. Lett.* **127**, 233201 (2021).
- [39] J. Hüpfel, F. Russo, L. M. Rachbauer, D. Bouchet, J. Lu, U. Kuhl, and S. Rotter, Continuity Equation for the Flow of Fisher Information in Wave Scattering (2023), [arxiv:2309.00010](https://arxiv.org/abs/2309.00010) [cond-mat, physics:physics, physics:quant-ph].
- [40] A. Fleming, C. Conti, and A. Di Falco, Perturbation of Transmission Matrices in Nonlinear Random Media, *Annalen der Physik* **531**, 1900091 (2019).
- [41] See Supplemental Material at [URL will be inserted by publisher].
- [42] M. Davy, M. Kühmayer, S. Gigan, and S. Rotter, Mean path length invariance in wave-scattering beyond the diffusive regime, *Commun Phys* **4**, 85 (2021).
- [43] P. Del Hougne, R. Sobry, O. Legrand, F. Mortessagne, U. Kuhl, and M. Davy, Experimental Realization of Optimal Energy Storage in Resonators Embedded in Scattering Media, *Laser & Photonics Reviews* **15**, 2000335 (2021).
- [44] D. L. Sounas and A. Alù, Fundamental bounds on the operation of Fano nonlinear isolators, *Phys. Rev. B* **97**, 115431 (2018).
- [45] M. Cotrufo, S. A. Mann, H. Moussa, and A. Alu, Nonlinearity-Induced Nonreciprocity—Part I, *IEEE Trans. Microwave Theory Techn.* **69**, 3569 (2021).
- [46] C.-Z. Wang, R. Kononchuk, U. Kuhl, and T. Kottos, Loss-Induced Violation of the Fundamental Transmittance-Asymmetry Bound in Nonlinear Complex Wave Systems, *Phys. Rev. Lett.* **131**, 123801 (2023).
- [47] P. Del Hougne, F. Lemoult, M. Fink, and G. Lerosey, Spatiotemporal Wave Front Shaping in a Microwave Cavity, *Phys. Rev. Lett.* **117**, 134302 (2016).
- [48] L. Chen, T. Kottos, and S. M. Anlage, Perfect absorption in complex scattering systems with or without hidden symmetries, *Nat Commun* **11**, 5826 (2020).
- [49] A. Yaghjian, Electric dyadic Green's functions in the source region, *Proceedings of the IEEE* **68**, 248 (1980).
- [50] Y. D. Chong and A. D. Stone, Hidden Black: Coherent Enhancement of Absorption in Strongly Scattering Media, *Phys. Rev. Lett.* **107**, 163901 (2011).

Supplemental Material for “Detecting and Focusing on a Nonlinear Target in a Complex Medium”

THEORY

We consider a system without free charges and no magnetisation so that the wave equation is given by

$$\nabla \times (\nabla \times \mathbf{E}) = -\mu_0 \partial_t^2 \mathbf{D}. \quad (\text{S1})$$

We can now split up the electric displacement field $\mathbf{D} = \epsilon_0 \epsilon \mathbf{E} + \mathbf{P}^{\text{NL}}$ into a linear part given by the relative electric permittivity ϵ and a polarisation part $\mathbf{P}^{\text{NL}}[\mathbf{E}]$, which is nonlinear in \mathbf{E} . We are now going to make use of the Green’s tensor G_ω of the linear system at frequency ω with outgoing boundary conditions, i.e.

$$\nabla \times (\nabla \times G_\omega)(\mathbf{r}, \mathbf{r}') - \frac{\omega^2}{c^2} \epsilon(\mathbf{r}) G_\omega(\mathbf{r}, \mathbf{r}') = 1 \delta(\mathbf{r} - \mathbf{r}'). \quad (\text{S2})$$

This definition allows us to rewrite the monochromatic solution of the wave equation at frequency ω using the Green’s tensor in the far field

$$\mathbf{E}_\omega(\mathbf{r}) = \mathbf{E}_\omega^{\text{L}}(\mathbf{r}) + \frac{\omega^2}{\epsilon_0 c^2} \int G_\omega(\mathbf{r}, \mathbf{r}') \mathbf{P}_\omega^{\text{NL}}[\mathbf{E}](\mathbf{r}') d\mathbf{r}', \quad (\text{S3})$$

where $\mathbf{E}_\omega^{\text{L}}$ describes the incident field scattered in the linear system (i.e. $\nabla \times (\nabla \times \mathbf{E}_\omega^{\text{L}}) + \frac{\omega^2}{c^2} \epsilon \mathbf{E}_\omega^{\text{L}} = 0$) and $\mathbf{P}_\omega^{\text{NL}}[\mathbf{E}]$ the nonlinear polarisation field corresponding to \mathbf{E}_ω . The nonlinear response is thus given by the second term.

Separating the linear and nonlinear contributions

Our first goal is going to be to separate these two contributions. For this we can make use of the fact that the linear scaling of the output field with the input field is broken due to the presence of the nonlinearity. We proceed by varying the strength (quantified by α) of the incident field $\mathbf{E}_\omega^{\text{L}, \text{in}} \rightarrow \mathbf{E}_\omega^{\text{L}, \text{in}} \alpha$, which produces a predictable linear response in the linear contributions of the scattered field $\mathbf{E}_\omega^{\text{L}, \alpha} = \mathbf{E}_\omega^{\text{L}} \alpha$. Therefore by varying α we can extract the nonlinear contributions of the field by removing exactly those contributions with linear scaling

$$\delta \mathbf{E}_\omega - \mathbf{E}_\omega \delta \alpha = \frac{\omega^2}{\epsilon_0 c^2} \int G_\omega(\mathbf{r}, \mathbf{r}') \left[\delta \mathbf{P}_\omega^{\text{NL}}(\mathbf{r}') - \mathbf{P}_\omega^{\text{NL}}[\mathbf{E}^\alpha](\mathbf{r}') \delta \alpha \right] d\mathbf{r}' \quad (\text{S4})$$

for $\delta \mathbf{E}_\omega = \mathbf{E}_\omega^{\alpha + \delta \alpha} - \mathbf{E}_\omega^\alpha$ and $\delta \mathbf{P}_\omega^{\text{NL}} = \mathbf{P}_\omega^{\text{NL}}[\mathbf{E}^{\alpha + \delta \alpha}] - \mathbf{P}_\omega^{\text{NL}}[\mathbf{E}^\alpha]$, whereby $\alpha, \alpha + \delta \alpha$ quantifies the strength of the incident field. This field now originates at the nonlinearity and propagates out of the system according to the Green’s tensor of the corresponding linear system. This already shows that a nonlinearity can be detected by observing the divergence of the outgoing field from the linear power scaling property. In the next section we are going to see how this can be exploited to create a focusing field on a point-like target.

Focusing on the nonlinearity

Our next objective will be to find an incident state that focuses onto the location of the nonlinearity. We reverse the outgoing field derived in the previous section so that the incident field is given by $\mathbf{E}_\omega^{\text{opt}} = (\delta \mathbf{E}_\omega - \mathbf{E}_\omega \delta \alpha)^*$ in the far field and creates a focus at the nonlinear dielectric. This can be seen for systems, where ϵ is real valued (i.e. no absorption or gain present) by using Green’s identity to identify the linear response $\mathbf{E}_\omega^{\text{L}, \text{opt}}$ of the system to the incident state $(\delta \mathbf{E}_\omega - \mathbf{E}_\omega \delta \alpha)^*$, i.e. a system with the nonlinearity removed,

$$\mathbf{E}_\omega^{\text{L}, \text{opt}}(\mathbf{r}_1) = \lim_{R \rightarrow \infty} \int_{S_R^3} [\mathbf{n} \times G_\omega^*(\mathbf{r}, \mathbf{r}_1)] \cdot [\nabla \times (\delta \mathbf{E}_\omega - \mathbf{E}_\omega \delta \alpha)(\mathbf{r})] - [\nabla \times G_\omega^*(\mathbf{r}, \mathbf{r}_1)] \cdot [\mathbf{n} \times (\delta \mathbf{E}_\omega - \mathbf{E}_\omega \delta \alpha)(\mathbf{r})] d\sigma, \quad (\text{S5})$$

where S_R^3 is the surface of a sphere with radius R centered at the origin and G_ω^* corresponds to the Green's function with incoming boundary conditions. We can simplify this expression by using the Green's function identity

$$\begin{aligned} -2i\text{Im}(G_\omega(\mathbf{r}_0, \mathbf{r}_1)) &= -2i \int_{S_R^3} (\nabla \times \text{Im}(G_\omega)(\mathbf{r}, \mathbf{r}_1)) \cdot (\mathbf{n} \times G_\omega(\mathbf{r}, \mathbf{r}_0)) - (\mathbf{n} \times \text{Im}(G_\omega)(\mathbf{r}, \mathbf{r}_1)) \cdot (\nabla \times G_\omega(\mathbf{r}, \mathbf{r}_0)) d\sigma \\ &= \int_{S_R^3} (\nabla \times G_\omega^*(\mathbf{r}, \mathbf{r}_1)) \cdot (\mathbf{n} \times G_\omega(\mathbf{r}, \mathbf{r}_0)) - (\mathbf{n} \times G_\omega^*(\mathbf{r}, \mathbf{r}_1)) \cdot (\nabla \times G_\omega(\mathbf{r}, \mathbf{r}_0)) d\sigma. \end{aligned} \quad (\text{S6})$$

The second equality holds due to the outgoing boundary condition of G_ω . Note that we avoided the ambiguity of the dyadic Green's function in the source region [S49] in Eq. (S5)/(S6) because $\mathbf{E}_\omega^{\text{L,opt}}$, $\text{Im}(G_\omega)$ are solutions of the source free wave equation inside the system.

This gives us the linear contribution of the field at the nonlinearities

$$\mathbf{E}_\omega^{\text{L,opt}}(\mathbf{r}) = -\frac{2i\omega^2}{\epsilon_0 c^2} \int \text{Im}G_\omega(\mathbf{r}, \mathbf{r}') \left[\delta \mathbf{P}_\omega^{\text{NL}}(\mathbf{r}') - \mathbf{P}_\omega^{\text{NL}}[\mathbf{E}^\alpha](\mathbf{r}') \delta\alpha \right] d\mathbf{r}'. \quad (\text{S7})$$

On the one hand this formula indicates that we can expect a field inside of the nonlinearity. However, on the other hand, the term $\text{Im}G_\omega(\mathbf{r}, \mathbf{r}')$ can deteriorate the focusing on the nonlinearity and we have so far not included the nonlinear response of the target, which will in general introduce difficulties in predicting the exact field. Nevertheless, these difficulties can be overcome for the case of point-like nonlinearities.

Point-like nonlinearity

We consider a singular nonlinearity in the Rayleigh regime with center at \mathbf{r}_0 volume D_R and diameter R , so that the far field is given by

$$\mathbf{E}_\omega(\mathbf{r}) = \mathbf{E}_\omega^{\text{L}}(\mathbf{r}) + \frac{\omega^2 D_R}{\epsilon_0 c^2} G_\omega(\mathbf{r}, \mathbf{r}_0) \mathbf{P}_\omega^{\text{NL}}[\mathbf{E}](\mathbf{r}_0). \quad (\text{S8})$$

Thus the outgoing field pattern is only given by the Green's tensor of the linear system $G_\omega(\mathbf{r}, \mathbf{r}_0)$ coupling the location of the nonlinearity to the far field. Based on this we can simplify Eq. (S7) giving us the linear contribution

$$\mathbf{E}_\omega^{\text{L,opt}}(\mathbf{r}_0) = -\text{Im}G_\omega(\mathbf{r}_0, \mathbf{r}_0) \frac{2i\omega^2 D_R}{\epsilon_0 c^2} \left[\delta \mathbf{P}_\omega^{\text{NL}}(\mathbf{r}_0) - \mathbf{P}_\omega^{\text{NL}}[\mathbf{E}^\alpha](\mathbf{r}_0) \delta\alpha \right]. \quad (\text{S9})$$

Thus in the linear reference system a focus can be created at the location of the nonlinearity.

FAR FIELD DESCRIPTION

We consider the case of scalar waves and a basis of the wavefronts in the far field \mathbf{E}_n so that the in- and outgoing fields have the corresponding coefficients \mathbf{c}^{in} , \mathbf{c}^{out} . In linear systems these coefficients can be connected by the linear scattering matrix S^{L} . However in our case this does no longer hold true due to the nonlinearity violating the superposition principle. Luckily, those incident fields that do not interact with the nonlinearity stay linear, which means that for a point-like nonlinearity an incident field quantified by \mathbf{d}^* can be found, so that all orthogonal incident fields do not interact with the nonlinearity. This incident field \mathbf{d}^* corresponds to the far field coefficients of $G_\omega(\mathbf{r}, \mathbf{r}_0)$ in our chosen basis, i.e. $d_j = \frac{-i}{2\omega} \int_{\partial\Omega} (\mathbf{n} \times \mathbf{E}_j^*(r)) \cdot (\nabla \times G_\omega(r, r_0)) - (\nabla \times \mathbf{E}_j^*(r)) \cdot (\mathbf{n} \times G_\omega(r, r_0)) d\sigma$, where Ω is the volume of the scattering system. Using Green's identity we can see that $d_j = \frac{i}{2\omega} (\mathbf{E}_j^{\text{L}})^*(\mathbf{r}_0)$, where \mathbf{E}_j^{L} corresponds to the solution of the linear system of the far field mode j . Thus if we take an incident state $\mathbf{c}^{\text{in}} \perp \mathbf{d}$ then the linear part of the field is given by $\mathbf{E}^{\text{L}}(\mathbf{r}_0) = \sum_j c_j \mathbf{E}_j^{\text{L}}(\mathbf{r}_0) \propto \mathbf{d}^\dagger \mathbf{c} = 0$, showing that no field is present at the location of the nonlinearity. With this in mind and due to the nonlinearity only depending on the linear field at \mathbf{r}_0 , we can now describe the scattering of the incident field using a nonlinear scattering operator $\mathbf{c}^{\text{out}} = \hat{S}[\mathbf{c}^{\text{in}}]$ so that

$$\hat{S}[\mathbf{c}^{\text{in}}] = S^{\text{L}} \mathbf{c}^{\text{in}} + \mathbf{d} f(\mathbf{d} \cdot \mathbf{c}^{\text{in}}), \quad (\text{S10})$$

whereby S^L is the scattering matrix of the linear system without the nonlinearity and f a nonlinear function. This nonlinear operator can now be probed using a basis of incident states, which can be conveniently summarized in the matrix S^α so that we have

$$S_{m,n}^\alpha = S_{m,n}^L + d_m \alpha^{-1} f(\alpha d_n), \quad (\text{S11})$$

where we choose the basis of incident states $c_k^{\text{in}} = \alpha \delta_{k,n}$ for all n , quantify the strength of the incident fields by α and normalize the outgoing fields by α . This has the advantage that for linear system this reduces to the scattering matrix, while we can probe the nonlinear contributions of the scattering operator by varying α . Note however that S^α does not fully describe the operator \hat{S} , due to the loss of the superposition principle, but only the response for a basis of incident states.

Extracting the focusing field

We will now apply Eq. (S4) to a basis of incident states for $\alpha, \alpha + \delta\alpha$ respectively. The results are summarized by the matrices $S^\alpha, S^{\alpha+\delta\alpha}$, which gives us

$$\Delta S_{m,n} = (S^{\alpha+\delta\alpha} - S^\alpha)_{m,n} = d_m ((\alpha + \delta\alpha)^{-1} f((\alpha + \delta\alpha) d_n) - \alpha^{-1} f(\alpha d_n)). \quad (\text{S12})$$

This rank-one matrix contains information of at least one incident state that interacts with the nonlinearity, allowing us to apply a singular value decomposition on ΔS to extract \mathbf{d} . Note that if multiple far field modes couple to the nonlinearity (e.g. non-scalar waves, multiple polarization degrees of freedom) or if multiple nonlinearities are present then the non-linearity acts on the subspace of these modes. In this case f would need to be replaced by a function describing the nonlinear interaction between these states and the rank of the matrix ΔS will be the dimension of this subspace. In general while we can still use ΔS to identify modes that focus on the nonlinearity, in order to create an optimal focus more information on the non-linearity is needed.

Reciprocity and nonlinearity detection

One important property in most linear systems is the reciprocity condition, which can now break due to nonlinear interactions. In our case this turns out to be

$$(S^\alpha - (S^\alpha)^T)_{m,n} = d_m \alpha^{-1} f(\alpha d_n) - d_n \alpha^{-1} f(\alpha d_m). \quad (\text{S13})$$

While in theory it is not guaranteed that we will see reciprocity breaking using S^α (e.g. if \mathbf{d} corresponds to a basis vector), in practice we saw that this can serve as a useful tool for the detection of the nonlinearity.

Lowest singular value and absorption

We find a strong average correlation between the wavefront for maximal focusing $\mathbf{c}^{\text{in}} = \mathbf{d}^*$ and the eigenvector \mathbf{U}_N corresponding to the smallest eigenvalue σ_N of $(S^\alpha)^\dagger S^\alpha$ that gives minimal reflection from the cavity and therefore maximal absorption [S50]. The correlation coefficient averaged over the frequency range is $\langle |\mathbf{U}_N^* \cdot \mathbf{c}^{\text{in}}| \rangle \sim 0.8$. As the cavity is closed, absorption at the target is indeed the main loss mechanism. The correlation coefficient is however below unity since other dissipative mechanisms such as uniform absorption within the cavity also takes place. Small eigenvalues $\sigma_N \rightarrow 0$ indicate that the incident energy is almost completely dissipated within the target.

CORRECTION OF THE PHASE FOR BROADBAND SIGNALS

The wavefront for optimal focusing in space and time corresponds to the time-reversed (or equivalently phase-conjugate) of the transmission coefficient $\mathbf{c}^{\text{opt}}(\omega) = \mathbf{t}^*(\omega)$. The phases at each frequency are aligned at the focus, meaning that the scattered wavefront $\mathbf{c}^{\text{opt}}(\omega) = \Delta S(\omega) \mathbf{c}^{\text{opt}}(\omega)$ acquires a phase equal to $\arg[t(\omega)]$. We therefore determine the phase $\phi(\omega)$ from the condition $\arg[\mathbf{c}^{\text{in}} e^{i\phi} \Delta S \mathbf{c}^{\text{in}} e^{i\phi}] = 0$. Because both $\mathbf{c}^{\text{in}} e^{i\phi}$ and $\mathbf{c}^{\text{in}} e^{i(\phi+\pi)}$ satisfy this condition, we finally exploit the continuity of $\phi(\omega)$ over the bandwidth to correct π -phase shifts.